JOURNAL OF MODERN OPTICS, 1997, VOL. 44, NO. 11/12, 2207–2225

Homodyne tomography of classical and non-classical light

G. BREITENBACH and S. SCHILLER

Fakultät für Physik M696, Universität Konstanz, D-78457 Konstanz, Germany. http://quantum-optics.physik.uni-konstanz.de

(*Received 28 January 1997; revision received 8 April 1997*)

Abstract. States with explicit quantum character, such as squeezed vacuum and bright squeezed light, as well as coherent states and incoherent superpositions of coherent states were generated and analysed by tomographical methods. Wigner functions, photon-number distributions, density matrices and phase distributions were reconstructed with high accuracy. Features such as photon number oscillations, sub-Poissonian and super-Poissonian photon statistics, bifurcations of the phase distribution, and loss of coherence were observed, demonstrating the usefulness of quantum state reconstruction as an analysing tool in quantum optics experiments.

1. Introduction

Quantum state reconstruction (QSR) is based on extracting the maximum accessible information on a state and processing it by appropriate algorithms to obtain its phase-space distribution function or density matrix [1]. Historically, states of the light field were the first on which QSR was performed. While the existence of non-classical states of the light field had been firmly established by the mid-1980s [2], the advent of QSR techniques has opened up a new perspective of such states. Initial investigations comprised pulsed squeezed vacuum [3, 4] and coherent states [5] and the photon statistics of pulsed semiconductor laser diodes [6]. QSR of light was subsequently extended to the continuous-wave regime, including squeezed vacuum with a high degree of quantum noise reduction [7, 8], and bright squeezed light [9]. Because of the rapid development of theoretical and numerical tools for quantum state analysis [10–14] on the one hand and modern data recording and processing equipment on the other hand, quasi-real-time quantum state observation is now possible. In this paper we review the results of QSR methods applied to non-classical light generated by an optical parametric amplifier (OPA) and to states of the light field with various degrees of coherence.

2. Homodyne tomography

To reconstruct a quantum state, a large number of measurements on an ensemble of identically prepared states has to be performed [15]. For the light field this is accomplished by balanced homodyning [16]. As shown later in figure 1, the signal wave is spatially overlapped at a 50–50 beam splitter with a strong coherent oscillator of nearly the same frequency. Subtracting the photocurrents of two detectors at the two beam-splitter output ports yields a current i_-, which is directly proportional to the measurement result of the signal's electric field

operator $E(\theta) \propto X_\theta = X\cos\theta + Y\sin\theta$ at a specific phase angle θ, where $X = (a + a^\dagger)/2^{1/2}$ and $Y = (a - a^\dagger)/2^{1/2}\mathrm{i}$ are the non-commuting quadrature operators. The angle θ is determined by the relative phase between the signal wave and the local oscillator. It is varied linearly in time by a moveable mirror in the beam path of the local oscillator. In this way the rapid oscillation of the free time evolution of the electric field operator $E(t) \propto X\cos(\omega t) + Y\sin(\omega t)$ is converted to a controlled phase dependence $E(\theta)$. Thus, assuming that the signal state (i.e. its density matrix) emitted by the source does not change during the measurement time, $i_-(t)$ furnishes an image of the time evolution of the signal's electric field with the corresponding fluctuations at each phase angle.

Although the recording of this noise current conveys an appealing depiction of the signal's quantum state, a concise description is obtained by determining the phase-space distribution functions and statistics in the photon number basis. To this end the recorded noise trace is divided into sections $[\theta, \theta + \Delta\theta]$, $\theta \in [0, 2\pi]$, in each of which the statistical distribution of the fluctuations of i_- is formed, that is the probability distribution $P_\theta(x_\theta)$ of the eigenvalues x_θ of the quadrature X_θ. These distributions are the projection integrals of the signal state's Wigner function $W(x, y)$ in rotated coordinates:

$$P_\theta(x_\theta) = \int_{-\infty}^{\infty} W(x_\theta\cos\theta - y_\theta\sin\theta, x_\theta\sin\theta + y_\theta\cos\theta)\,\mathrm{d}y_\theta, \qquad (1)$$

where $y_\theta = -x\sin\theta + y\cos\theta$. The Wigner function is obtained from the set $\{P_\theta(x_\theta)\}$ by backprojection via use of the inverse Radon transform [10].

The alternative reconstruction method that we apply below yields the elements ρ_{nm} of the density matrix in the Fock basis via integration of $\{P_\theta\}$ over a set of pattern functions which have been described in detail in [11]. This method does not introduce any data filtering and offers in principle the possibility of 'on-line' reconstruction, that is to process each data point directly after being recorded.

3. The experiment

A schematic diagram of the experiment is shown in figure 1. As laser source we employ a miniature monolithic Nd-doped yttrium aluminium garnet laser (1064 nm; 500 mW; Lightwave model 122). To reduce the excess noise of the laser due to the relaxation oscillations, the laser beam traverses a high-finesse ($\mathcal{F}$ = 10 400) mode-cleaning cavity with a linewidth of 170 kHz. It is then split into three parts and directed as the local oscillator to the homodyne detector, to the frequency doubler to generate the pump wave for the OPA, and to injection-seed the OPA. Filter cavity and frequency doubler lengths are locked to the laser frequency by a frequency modulation technique. Three isolators (not shown in the schematic diagram) prevent back reflection of the laser light from the filter cavity into the laser, from the standing-wave frequency doubler into the filter cavity or from the OPA into the frequency doubler.

The signal wave emitted from the OPA cavity and the local oscillator wave are Gaussian TEM_{00} waves. Their waists are carefully matched to 99% at the beam splitter of the homodyne detector. The basic property of the homodyne detection system is a narrow-band detection of the electric field fluctuations at frequencies offset from the local oscillator frequency w by Ω = 1·5–2·5 MHz, rather than at dc, to avoid technical noise at low frequencies. The photodetectors contain passivated

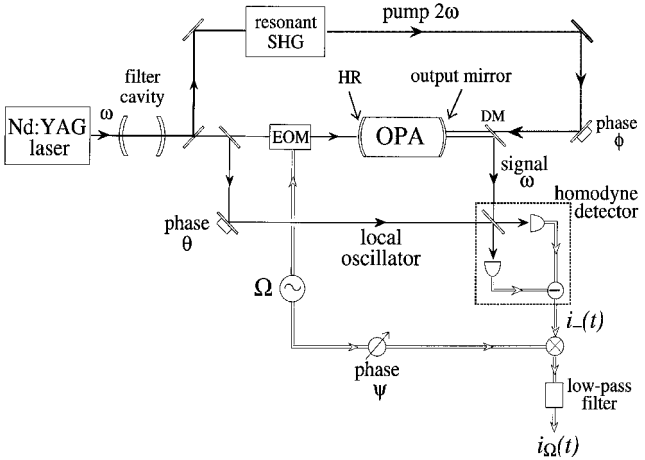

Figure 1. Experimental scheme for generating bright squeezed light and squeezed vacuum with an OPA: EOM, electro-optic modulator; DM, dichroic mirror; SHG, second-harmonic generator; Nd: YAG laser, Nd-doped yttrium aluminium garnet laser; HR, high reflector.

Epitaxx InGaAs photodiodes with removed front covers, exhibiting a quantum efficiency of 97% The photocurrents are amplified by transimpedance amplifiers with more than 30 MHz bandwidth. One part of the difference photocurrent is directed to a spectrum analyser for variance measurements; the other part is further amplified by a low-noise 40 dB gain amplifier and then mixed with an electrical oscillator of frequency Ω. The intermediate-frequency output of the mixer is further amplified and low-pass filtered by a SRS 560 low-noise amplifier. The bandwidth is set to 100 kHz, defining the bandwidth within which the fluctuations of i_- are detected. They are subsequently recorded by a 12 bit high-speed JMTEC analogue-to-digital (A/D) board. A trace of i_- with the phase θ scanned over 2π in 0·2 s contains about 500 000 points. Immediately after the data are stored in the on-board memory of the A/D converter, the probability distributions are sampled with 128 angle bins and 256 amplitude bins, and the numerical reconstructions are performed resulting in an overall reconstruction time of about 20 s.

3.1. *Squeezed vacuum generation by a subthreshold optical parametric oscillator*

The OPA employed consists of a monolithic standing-wave cavity, made of magnesium-oxide-doped lithium niobate. The OPA is operated in degenerate mode, that is the resonance frequency of the cavity mode is half the frequency of the pump wave, and the parametric gain of the nonlinear crystal is maximized via its temperature for the given pump frequency. The excellent free-running frequency stability of the laser, the dimensional stability of the OPA cavity and its broad linewidth of $\Gamma = 17$ MHz (half-width at half-maximum) allow stable operation of the experiment without active stabilization of the laser frequency to the OPA cavity resonance, relative drifts being less than 10 MHz min^{-1}.

The pump power beyond which the OPA becomes an oscillator is $P_{\mathrm{th}} = 28$ mW. Operated below threshold, the OPA is a source of squeezed vacuum. The predicted variances of the quantum fluctuations of the two quadratures with

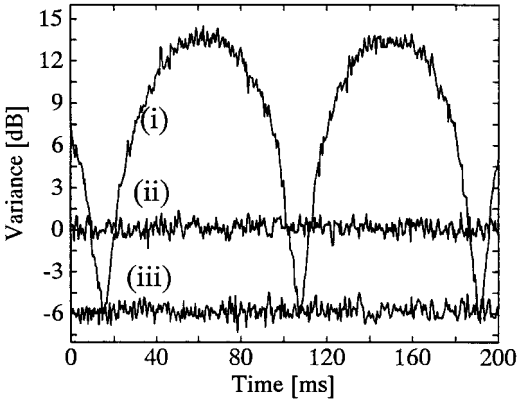

Figure 2. Squeezed vacuum from the monolithic OPA: trace (i), $\mathrm{Var}(X_\theta)$ against the phase of the local oscillator θ scanned over 2π in 200 ms; trace (iii), $\mathrm{Var}(X_\theta)$ with the phase θ fixed manually for minimum noise resulting in an averaged variance $\mathrm{Var}(X_{sq}) = 6 \pm 0{\cdot}25$ dB (0·25) below the vacuum level. The shot noise level is the average of trace (ii). The resolution bandwidth was 100 kHz, and the video bandwidth 1 kHz.

minimum (squeezed)/maximum (antisqueezed) noise have a Lorentzian spectrum given relative to the variance of vacuum by [17]

$$\mathrm{Var}\left[X_{\mathrm{sq/as}}(\Omega)\right] = 1 \mp \eta_e \frac{4(P_p/P_{th})^{1/2}}{\left[1 \pm (P_p/P_{th})^{1/2}\right]^2 + (\Omega/\Gamma)^2}, \tag{2}$$

where P_p is the pump power and $\eta_e = T_o/(T_o + T_{HR} + A) = 0{\cdot}88$ is the cavity escape efficiency, with $T_o = 2{\cdot}1\%$ being the transmission of the output mirror, $T_{HR} < 0{\cdot}05\%$ the transmission of the high reflector (HR) mirror, and $A = 0{\cdot}3\%$ the internal losses. With these values a maximum of $-7{\cdot}6$ dB (0·18) noise reduction below the vacuum (shot) noise level should be obtainable, for our detection efficiency of $94 \pm 2\%$ As shown in figure 2, in practice we reach a maximum value of $-6{\cdot}0 \pm 0{\cdot}25$ dB (0·25). Together with [18], this is the highest value for quadrature squeezing published so far. We believe that the discrepancy compared with the maximum achievable value is mainly due to the classical noise of the pump wave which is not completely removed by the filtering cavity. This is indicated by the presence of modulation signals of the frequency doubler in the OPA output spectrum and by the degradation of squeezing when the pump power approaches the OPO threshold. In this regime the measured values deviate from equation (2).

3.2. *Bright squeezed light generation by parametric amplification and deamplification*

A central aspect of our reconstruction experiments is the generation of bright squeezed light, that is with a coherent excitation in the sidebands at the frequency Ω where the measurements of the squeezed vacuum were performed. An efficient method to achieve this consists of using the OPA in a dual-port configuration [19]; we inject a phase-modulated 1064 nm wave into the HR mirror and extract the bright squeezed light from the output port, whose transmissivity $T_o \gg T_{HR}$.

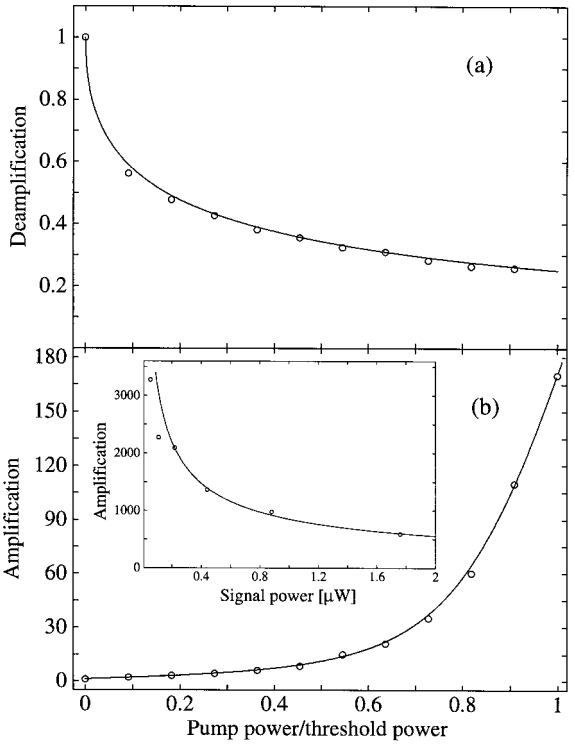

Figure 3. Parametric (*a*) deamplification and (*b*) amplification of a weak signal injected into the OPA: (——), theory; (°), measured values. The signal input power in (*b*) amounted to $P_{in} = 40\,\mu W$. The inset shows the maximum amplification against signal input power at constant pump power $P_p \approx P_{th}$.

Consider first the carrier (power P_{in} at ω) of the seed wave, on resonance with the cavity, and let $P_s = 4P_{in}T_oT_{HR}/(T_o + T_{HR} + A)^2$ be the output power transmitted by the OPA cavity through the T_o mirror in absence of the pump. Once the pump is turned on, the output power is gP_s with a gain g which depends on the power and the phase of the pump. Applying the standard treatment of nonlinear optical resonators, the strongest deamplification factor is found as

$$g_{min} = \frac{1}{\left[1 + (P_p/P_{th})^{1/2}\right]^2}. \tag{3}$$

Note that it is independent of the seed power and not explicitly dependent on the mirror transmissivities. Figure 3(*a*) shows agreement of this expression with the experimentally measured g_{min}. The maximum amplification g_{max}, on the other hand, depends on seed power since it is limited by depletion of the pump. At a fixed seed power the measured maximum gain as a function of pump power is shown in figure 3(*b*). By reducing the seed power the amplification factor can be increased. The inset of figure 3(*b*) shows this dependence with $P_p = 0{\cdot}985P_{th}$. Amplification factors up to 3260 were obtained. With a pump power exactly at threshold, the maximum gain is given by $g_{max} = (4\eta_e P_{th}/P_s)^{2/3}$.

Turning to the quantum fluctuations, we note and confirmed experimentally, that the spectrum of the quantum noise around Ω is not changed by the injection of the 100 pW seed beam, since the seed wave's fluctuations at Ω are at the vacuum limit owing to its low power the use of the filter cavity and because $T_{HR} \ll T_O$. To realize a coherent excitation at the measurement frequency Ω, we have to transfer a part of the optical power of the seeding input to sidebands at Ω. This is accomplished by a phase modulator placed before the OPA cavity driven at frequency Ω with a modulation index $\beta < 1$ (electro-optic modulation of the nonlinear crystal is also possible). The amplitude βE_0 of the sidebands is thus determined both by the relative phase ϕ of the pump wave and by the modulation index.

The Fourier components of the output field's quadratures can be written as

$$\begin{aligned} X(\Omega') &= E_0\delta(\Omega') + \beta E_0\left[\delta(\Omega' - \Omega) - \delta(\Omega' + \Omega)\right] + X_n(\Omega'), \\ Y(\Omega') &= Y_n(\Omega'). \end{aligned} \tag{4}$$

X_n and Y_n are the contributions stemming from the quantum noise entering and leaving through the OPA's output coupler. Their variances are functions of the optical phase ϕ between seed and pump wave, since the latter amplifies the in-phase fluctuations and deamplifies the out-of-phase fluctuations. By controlling the phase ϕ by a mirror attached to a piezoelectric actuator and the modulation index β, light of arbitrary amplitude squeezed in any arbitrary quadrature can be generated.

The homodyne detector output current i_- is mixed with an electrical local oscillator $\sim \sin(\Omega t + \psi)$, phase locked to the modulation source, and then low-pass filtered with 100 kHz bandwidth. The resulting current is

$$\begin{aligned} i_\Omega(\theta, t) \sim\ & \left\{\left[X_n(\Omega, t) + X_n(-\Omega, t)\right]\cos\theta - \left[Y_n(\Omega, t) + Y_n(-\Omega, t)\right]\sin\theta\right\} \\ & \times \sin\psi + \left\{\left[2\beta E_0 + X_n(\Omega, t) - X_n(-\Omega, t)\right]\sin\theta + \left[Y_n(\Omega, t)\right.\right. \\ & \left.\left. - Y_n(-\Omega, t)\right]\cos\theta\right\}\cos\psi, \end{aligned}$$

where $X_n(\Omega, t)$ and $Y_n(\Omega, t)$ are the quantum fluctuations in a 100 kHz wide band centred at Ω, transferred to dc. Setting the phase of the electric local oscillator such that $\cos\psi = 1$ and varying the local oscillator phase θ linearly in time, the mean homodyne current $\langle i_\Omega(\theta, t)\rangle \propto 2\beta E_0 \sin\theta$ oscillates harmonically and exhibits in addition phase-dependent fluctuations with the chosen bandwidth of 100 kHz.

4. Determining the quantum state

4.1. *Measurements of quantum noise*

The first step in QSR consists in determining the standard deviation ΔE_{vac} of the electric field of the vacuum state, to use it for the calibration of the noise of all generated states. Its value is obtained by a measurement of the noise current i_Ω with the homodyne detector signal input blocked. It serves as the unit of measurement for the electric field E_0 of the signal wave (or more precisely of its side bands $e_0 = 2\beta E_0$ at Ω).

A useful test of the measurement system is the verification of the independence of the variance of the coherent states' electric field from the degree of coherent excitation. This is demonstrated by the traces shown in figure 4. The angle-independent variance is equal to $(\Delta E_{vac})^2$ for all three traces. The methods

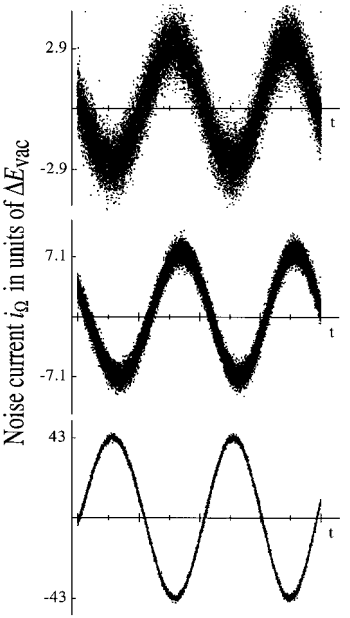

Figure 4. Noise traces i_Ω for three coherent states with different amplitudes e_0. Average photon numbers $\langle n \rangle = e_0^2/2$ from top to bottom are equal to 4·2, 25·2 and 924·5.

employed in our experiment allow us to detect coherent states of almost arbitrary field strength as long as the power of the signal beam is small in comparison with the local oscillator power. Accurate reconstructions are, however, limited to states with average photon numbers up to 40 ($e_0 < 9$), since the resolution of the A/D board is limited.

Figure 5 shows the recorded noise traces of different squeezed states generated by the OPA as well as the reference trace of the vacuum.† The minimum and maximum variances for the corresponding quadrature probability distributions P_θ are $\mathrm{Var}\left[X_{sq}(\Omega)\right] = -6\,\mathrm{dB}$ (0·25-fold noise suppression) and $\mathrm{Var}\left[X_{as}(\Omega)\right] = 14{\cdot}3\,\mathrm{dB}$ (26·9-fold noise enhancement) for the squeezed vacuum, in agreement with the measurement in figure 2, $\mathrm{Var}\left[X_{sq}(\Omega)\right] \approx -5\,\mathrm{dB}$, $\mathrm{Var}\left[X_{as}(\Omega)\right] \approx 13\,\mathrm{dB}$ for the bright squeezed states.

Not only the variance, the second-order statistical moment, can take values below that of the vacuum field, but also the higher-even-order statistical moments, as Hong and Mandel [20] predicted in 1985. Having sampled the complete distributions $\{P_\theta\}$, this higher-order squeezing of a quantum field is readily verified in our experiment up to the ten'ths statistical moment.

4.2. *Phase-space distributions*

Applying the inverse Radon transform to the sets of probability distributions $\{P_\theta\}$ yields the Wigner functions presented in figure 6. They are in agreement with the theoretical expression for bright non-minimum-uncertainty squeezed states, given by

† A video, showing the time evolutions of the quantum states presented here, can be obtained from the authors.

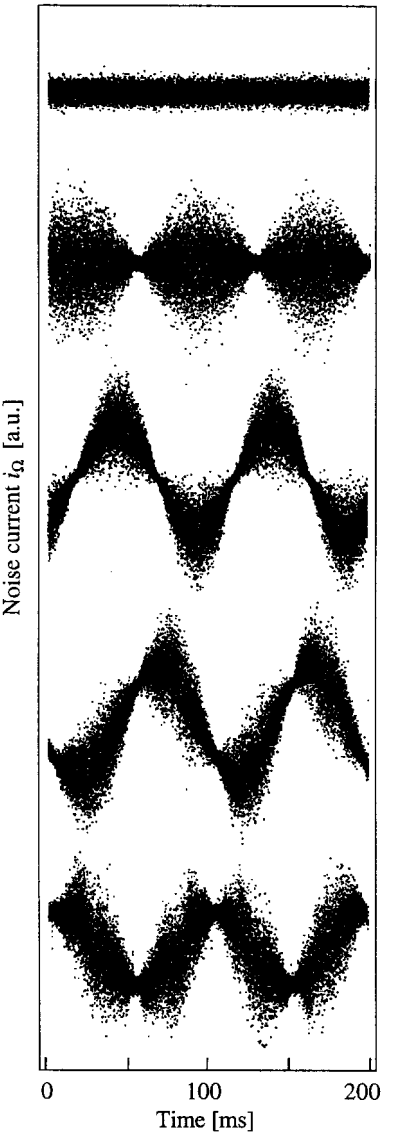

Figure 5. Noise traces i_Ω of the generated quantum states as a function of time (a.u., arbitrary units). From the top, vacuum state, squeezed vacuum state, phase-squeezed state, state squeezed in the $\phi = 48^\circ$ quadrature, and amplitude-squeezed state. The degree of squeezing was - 6 dB (0·25) for the squeezed vacuum, between - 5·2 and - 4·9 dB (between 0.3 and 0·32) for the bright squeezed states. The degrees of antisqueezing amounted to 12–14 dB (15·8–26·9).

$$W(x,y) = \frac{1}{\pi ab}\exp\left(-\frac{(x - e_0\cos\phi)^2}{a^2} - \frac{(y - e_0\sin\phi)^2}{b^2}\right), \tag{5}$$

where $x = x_0\cos\phi + x_{\pi/2}\sin\phi$, $y = -x_0\sin\phi + x_{\pi/2}\cos\phi$ are the phase-space coordinates used in standard textbooks, and $a = \{\mathrm{Var}[X_{\mathrm{sq}}(\Omega)]\}^{1/2}$, $b = \{\mathrm{Var}[X_{\mathrm{as}}(\Omega)]\}^{1/2}$ are the minimum and maximum standard deviations of the

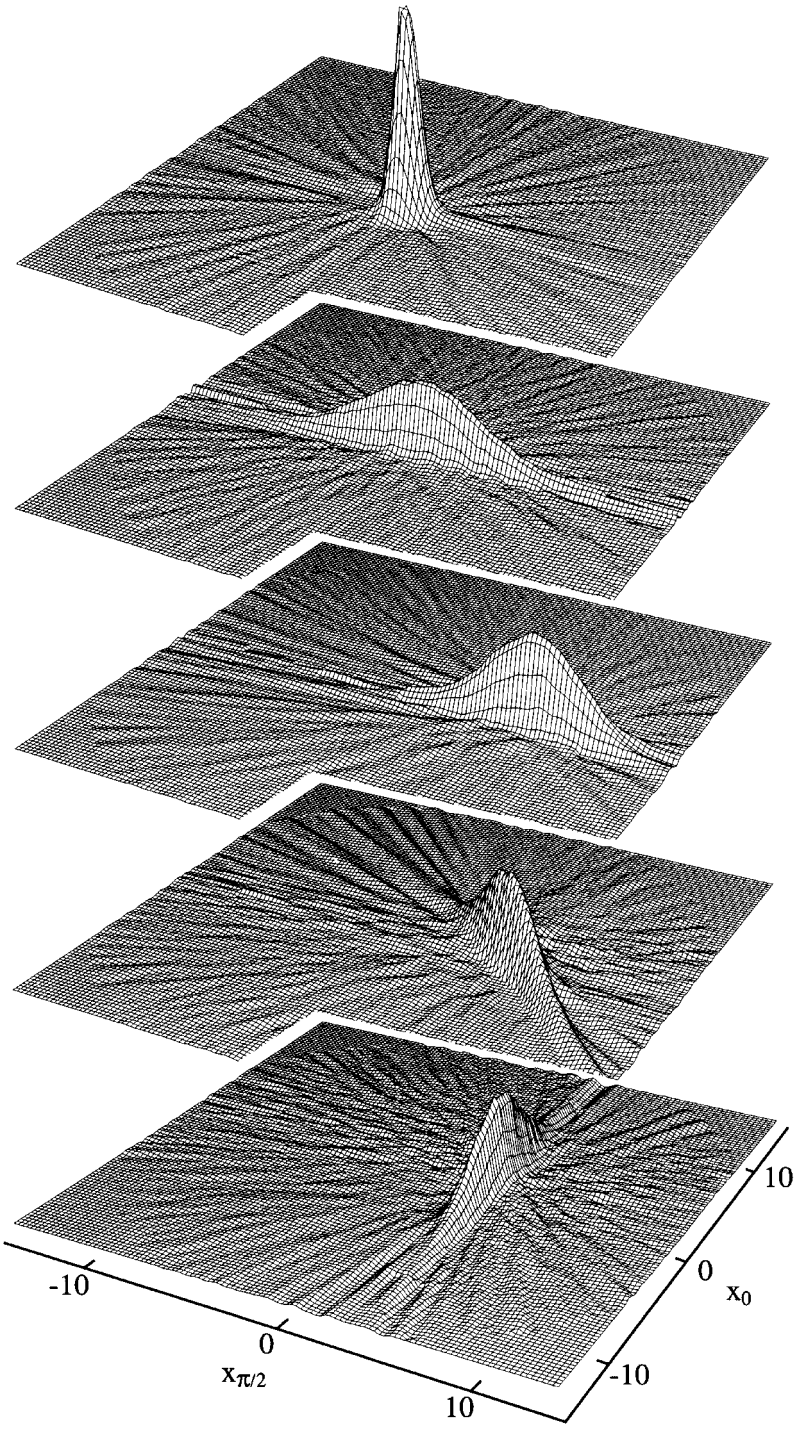

Figure 6. Reconstructed Wigner functions for the states in figure 5. From the top, vacuum state, squeezed vacuum state, phase-squeezed state, state squeezed in the $\phi = 48^{\circ}$ quadrature, and amplitude-squeezed state. The ripples at the base of all reconstructions are due to the finite number of angular divisions of the noise trace.

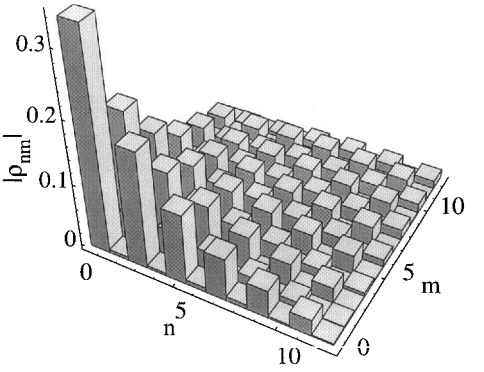

Figure 7. Reconstructed density matrix of the squeezed vacuum state in figure 5. The diagonal and the near off-diagonals exhibit strong odd–even oscillations, which can be explained by quantum interference in phase space. Every other off-diagonal is zero, owing to the inversion symmetry of the state's phase-space distribution.

quadrature fluctuations. For the bright squeezed light it can be clearly seen how a change in the angle ϕ between pump and OPA input signal corresponds to a rotation of the squeezed Wigner function in phase space.

It is important to note that, owing to non-unity detection efficiency η, the above reconstruction does not exactly yield the Wigner function but the s-parametrized phase-space distribution function $W(x,y,s)$ [21], with the parameter s given by $s = 1 - 1/\eta$, ($W(x,y,-1)$ represents the Q function, and $W(x,y,0)$ the original Wigner distribution). Therefore the quantum efficiency of the detection system is a crucial issue in any QSR experiment [22]. For our set-up it amounted to $94 \pm 2\%$, resulting in an s parameter of $-0{\cdot}064$. A second issue to be aware of when using the inverse Radon transform is that it contains a filtering process within the numerical algorithm which reduces the faithfulness of the reconstruction. If the filtering procedure is based on a quadratic regularization method with factor ε as described in [23], the influence of the data filtering can be determined quantitatively. It corresponds to a convolution of the Wigner function with a Gaussian of width $(2\varepsilon)^{1/2}$. Since detection losses result in a convolution of the Wigner function with a Gaussian as well, both influences are directly comparable. In our reconstructions the s parameter changed from $-0{\cdot}064$ (detection loss) to $-0{\cdot}072$ (detection loss + filtering). Thus, distortions due to the filtering process are negligible in our experiment and our reconstructed distributions are in fact very close to the states' Wigner function.

4.3. *Density matrices in the Fock basis*

The density matrix in the Fock representation is gained from the measured distributions via the integral

$$\rho_{nm} = \int \mathrm{d}\theta \, \mathrm{d}x_\theta \, P_\theta(x_\theta) \exp\left[\mathrm{i}(n - m)\theta\right] f_{nm}(x_\theta), \tag{6}$$

where the f_{nm} are the pattern functions described in [11]. The reconstructed density matrix of the squeezed vacuum is shown in figure 7. The odd–even oscillations in the diagonal and even off-diagonals are a striking evidence of the

two-photon down-conversion process [8]. A detailed analysis of the oscillatory character of the density matrix elements of non-minimum-uncertainty squeezed vacuum states, and its relation to phase space interference [24] can be found in [25]. An estimate for the upper limit of the experimental reconstruction error of 0·01 is given by the largest density matrix element (except ρ_{00}) of the reconstructed vacuum state. Within this error limit the reconstructed density matrix agrees with its theoretical estimation up to $n = 12$.

The photon-number distribution of the squeezed vacuum state, given by the diagonal elements ρ_{nn} is, as expected, strongly super-Poissonian, that is $\mathrm{Var}(n) > \langle n \rangle$. In general, for squeezed states that exhibit large antisqueezing $b^2 \gg 1$ and a relatively weak coherent excitation e_0, such as those presented in the previous paragraph, the photon statistics are super-Poissonian. This becomes apparent from the expressions for the photon-number average and variance of general squeezed states described by the Wigner function of equation (5) [26]:

$$\langle n \rangle = \frac{a^2 + b^2 - 2}{4} + \frac{e_0^2}{2}, \tag{7}$$

$$\mathrm{Var}(n) = \frac{a^4 + b^4 - 2}{8} + \frac{e_0^2}{2}(a^2 \cos^2 \phi + b^2 \sin^2 \phi). \tag{8}$$

These expressions were confirmed for the states of figure 5, by reconstruction of the corresponding photon-number distribution [9].

To obtain sub-Poissonian amplitude-squeezed light, we reduced the anti-squeezing (with a corresponding reduction in squeezing) by reducing the pump power of the OPA. Figure 8 shows the reconstructed density matrices of a sub-Poissonian amplitude-squeezed state and a super-Poissonian phase-squeezed state of approximately the same amplitude. The good agreement with the theoretical expectation is demonstrated in figure 9, which depicts the elements ρ_{nn} of these two matrices together with their theoretical counterparts, in comparison with those of a coherent state. The Mandel Q parameter for the sub-Poissonian photon statistics is to our knowledge the lowest value achieved so far for non-classical light generated by nonlinear frequency conversion [27].

This data analysis may be extended with the goal of improvement by taking into account the detection efficiency in our algorithms, thus trying to reconstruct the photon statistics of the signal *before* detection. This is done by applying the inverse Bernoulli transform to the reconstructed photon statistics using as parameter the detection efficiency [28]. We found that for our data the errors increase very rapidly even for small photon numbers n. The analysis of a squeezed vacuum state of our experiment by more powerful reconstruction methods employing Bayesian analysis has been described in [14].

To relate the values found for the average occupation number $\langle n \rangle$ to the actually measured powers, we note that $\langle n \rangle$ is the average photon flux per unit bandwidth. Given our detection bandwidth of 100 kHz set by the low-pass filter, a state with $\langle n \rangle$ photons implies a total photon flux of $\langle n \rangle 10^5$ photons $s^{-1} \approx 0{\cdot}02 \langle n \rangle$ pW power distributed over the side bands 100 kHz wide at $\pm\Omega$. For a coherent state this light power is concentrated in the coherent excitation e_0. For a bright squeezed state the flux in the side bands arises partly from the monochromatic coherent excitation, and partly from the wide-band (and, on the scale of 100 kHz, white) noise power of the quantum fluctuations.

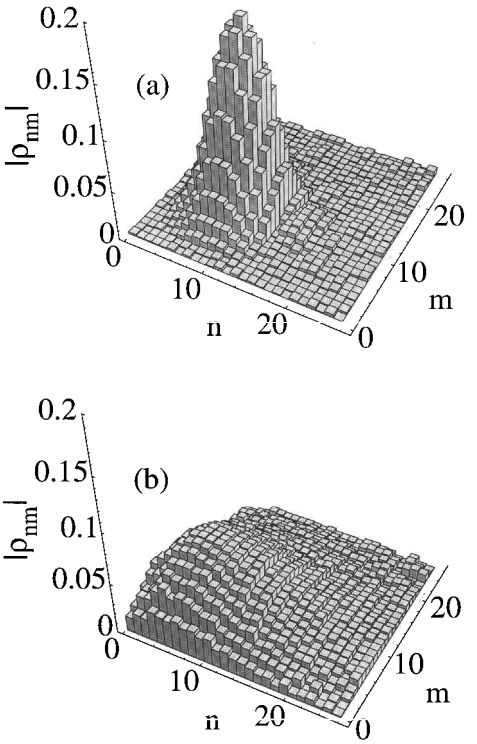

Figure 8. Reconstructed density matrices (absolute values) of (*a*) an amplitude-squeezed state and (*b*) a phase-squeezed state with approximately equal amplitude $e_0 = 4{\cdot}12$, squeezed variance $a^2 = 0{\cdot}44$ and antisqueezed variance $b^2 = 3{\cdot}4$. The deviation of the matrix elements from the theoretical values is of the order of 0·01.

The total output power of the OPA consists of the transmitted seed wave power, $P_s \approx 100\,\mathrm{pW}$, plus the wide-band contribution of the quantum fluctuations. Integration over the squeezing spectrum of equation 2 results in a contribution $2\eta_{es}\Gamma\pi P_p/(P_{th} - P_p) = 6{\cdot}5 \times 10^8$ photons $s^{-1} \approx 100\,\mathrm{pW}$ if $P_p = 0{\cdot}9P_{th}$. Thus the total output power is about 200 pW.

Another important feature of a quantum state that can be read off its density matrix is the purity. The trace of the square of the density matrix is a measure of the deviation of the state from a pure one. For the states in figure 8 this value amounted to $\mathrm{Tr}\,\rho^2 = 0{\cdot}82$–$0{\cdot}85$ in agreement with the theoretical value given by $1/ab$. For the stronger squeezed states in figure 6 the agreement of $\mathrm{Tr}\,\rho^2 \approx 0{\cdot}39$ with $1/ab \approx 0{\cdot}45$ is reduced, since Fock states with high n contribute significantly to ρ but could not be accurately reconstructed from the data. That in general for the generated squeezed states the value $\mathrm{Tr}\,\rho^2 = 1/ab$ is smaller than the values expected for the given high overall detection efficiency is because the states' mixed character is also caused by additional noise of the pump beam.

4.4. *Phase distributions*

The definition of a quantum-mechanical phase operator has been a subject of intense interest in the quantum optics community [29]. Several possible definitions exist, which are equally well usable from the point of view of QSR, as has been

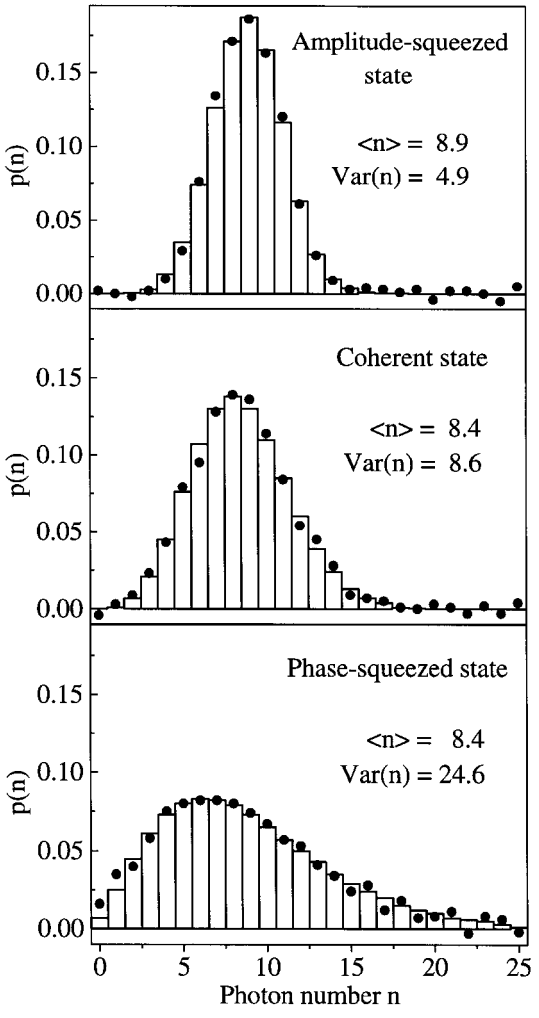

Figure 9. Photon number distribution of the states in figure 8 in comparison with a coherent state of the same amplitude: (•), experimental data; histograms show the theory. The amplitude-squeezed state shows a strong sub-Poissonian statistics. The deviation of photon number average and variance from their theoretical expectations is less than 2%

shown by a comparison of different phase operators by Beck *et al.* [30]. The Pegg–Barnett phase distribution, defined by

$$P_{pb}(\theta) = \frac{1}{2\pi} \sum_{n,m=0}^{s} \exp\left[\mathrm{i}(m - n)\theta\right] \rho_{nm} \tag{9}$$

on the $(s + 1)$-dimensional subspace spanned by $\{|n\rangle\}_{n=0,\ldots,s}$ is a convenient choice for analysing the measured states' phase distributions, since by QSR it is only possible to determine a finite number of density matrix elements ρ_{nm}. In the same way as the photon number distribution is the appropriate representation to verify intensity squeezing for amplitude-squeezed light, the phase distribution is in-

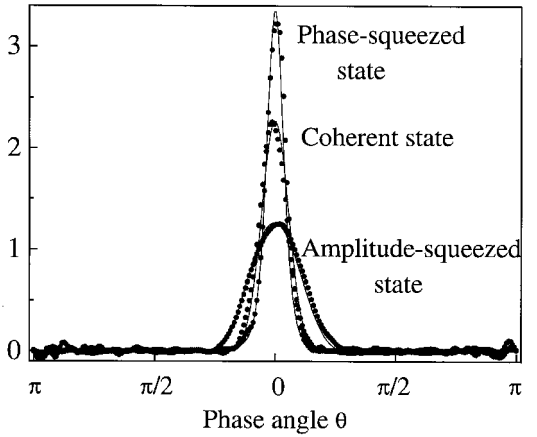

Figure 10. Pegg–Barnett phase distribution for the states in figure 8 in comparison with a coherent state of the same amplitude: (•), experimental data; (——), theoretical expectations.

tended to accomplish the same for the phase-squeezed states. Figure 10 shows the phase distributions for the states in figure 8, demonstrating the phase squeezing and antisqueezing of these states in comparison with a coherent state of the same amplitude [31] (new numerical concepts for direct reconstruction of the Susskind–Glogower phase distribution have been presented in [32]).

As the coherent excitation e_0 of the amplitude-squeezed state is reduced, a bifurcation of the phase distribution occurs (figures 11 (*a*) and (*b*)). Finally the squeezed vacuum with $e_0 = 0$ displays a striking double-peaked phase distribution (figure 11 (*c*)) due to the large ratio of the antisqueezed to the squeezed variance. This behaviour was first pointed out by Schleich *et al.* [33].

4.5. *Quantum state reconstruction of incoherent superpositions of coherent states*

As a demonstration of the applicability of QSR to more general states of the light field and to investigate the influence of noise on the measurement system, we studied coherent states with controlled addition of classical noise.

In contrast with noise suppression below the vacuum level, the addition of noise to an experimental system is one of the easiest tasks to be accomplished in the laboratory. With the set-up used to study coherent states (pump off), phase noise was added to the signal wave by applying a random modulation (Gaussian noise of 1 MHz bandwidth) and, to achieve stronger modulation amplitudes, an additional 2 kHz sine wave to a piezo-mounted mirror in the signal wave's path before the OPA cavity. Changing the amplitude of the modulation from zero up to one optical wavelength controls the degree of phase diffusion of the state. Amplitude noise was added to the signal wave by modulating with Gaussian noise the amplitude of the rf source driving the phase modulator that generated the side bands at the measurement frequency Ω. 'Thermal' noise was implemented by combining these two noise sources or by passing the seed wave through a rapidly rotating transparent wheel having a rough surface so that random scattering occurs. The latter method had been used as early as 1965 by Arecchi [34] in one of the first experiments on optical quantum state characterization.

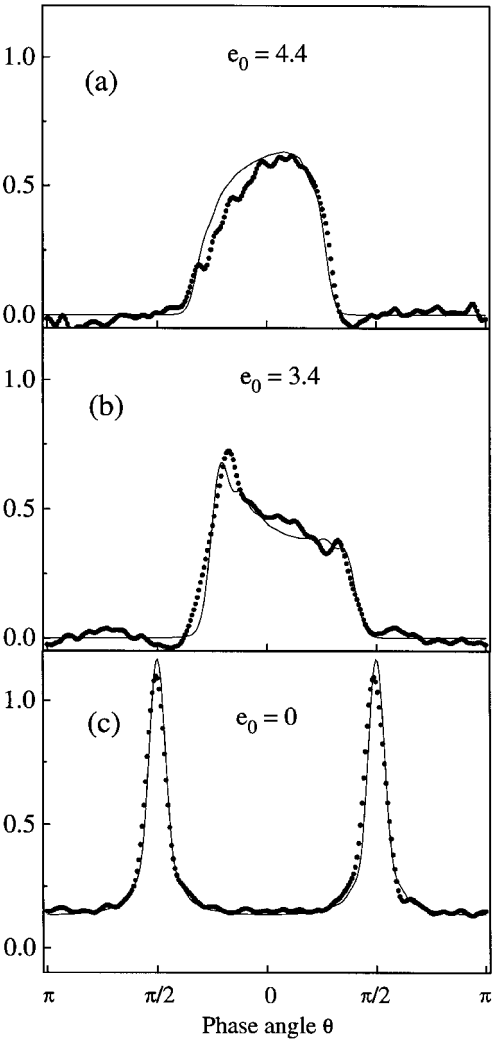

Figure 11. Pegg–Barnett phase distribution for two amplitude-squeezed states with amplitudes e_0 (*a*) before and (*b*) after the bifurcation point,where the two maxima of the phase distribution split; (*c*) the squeezed vacuum state in figure 5: (•), experimental data; (——), to theory. The slight asymmetries are due to a variation of the squeezing angle ϕ, since it was not actively stabilized.

The noise traces of the states and the Wigner functions of the phase-diffused states are shown in figures 12 and 13 (similar states have been reported in [35]). Since the amplitude-diffused state's distribution is very similar to that of a phase-squeezed state, it is not presented here. The completely phase-diffused coherent state has been described in [36]. Its ring-shaped, clearly non-Gaussian Wigner function is given by [37]

$$W(x,y) = \frac{1}{2\pi}\exp(-x^2 - y^2 - e_0^2) I_0\left[2e_0(x^2 + y^2)^{1/2}\right], \tag{10}$$

where I_0 is the modified Bessel function of order zero.

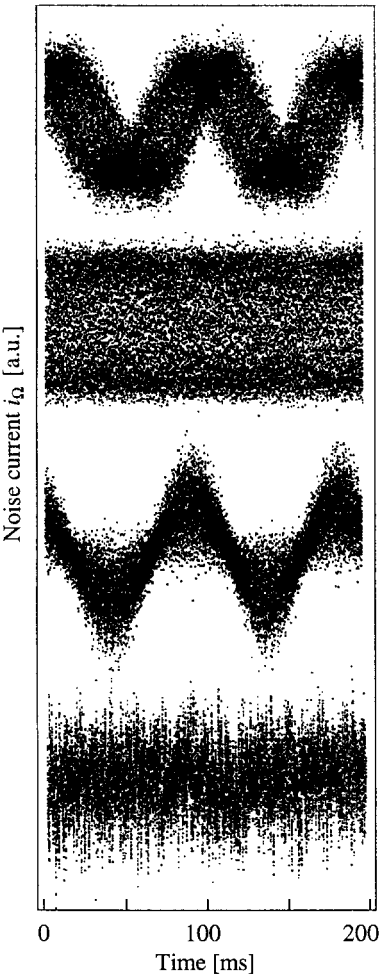

Figure 12. Noise traces i_Ω of incoherent superpositions of coherent states as a function of time (a.u., arbitrary units). From the top, partially phase-diffused state, completely phase-diffused state, amplitude-diffused state ($a^2 = 1{\cdot}0$; $b^2 = 5{\cdot}4$) and thermal state ($a^2 = b^2 = 14{\cdot}8$).

The coherence properties of the generated states are best visualized by the density matrix in the Fock representation. Figure 14 shows how the addition of phase noise to the coherent state leads to an increasing extinction of its off-diagonal elements, while the diagonal elements, that is the Poissonian statistics, remain unchanged. The thermal state, on the other hand, exhibits an exponential decay of the diagonal elements and off-diagonal elements that are zero within the experimental error of 0·01.

5. Conclusion

Quantum state analysis of light by homodyne tomography has been developed into a reliable and easily applicable tool for the investigation of single-mode light

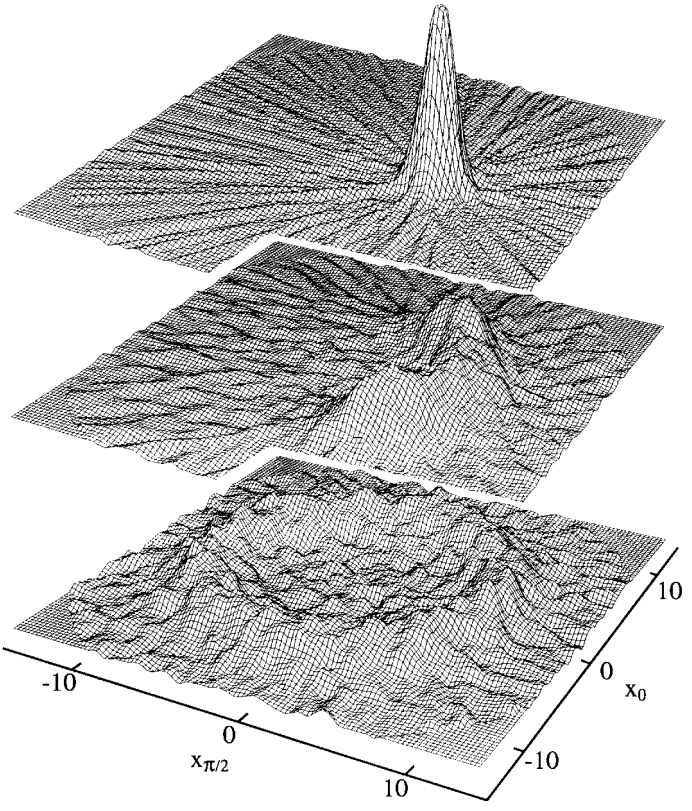

Figure 13. From the top, reconstructed Wigner function of a coherent state, a partially phase-diffused state, and a completely phase-diffused state.

sources. Owing to the high detection efficiency achievable and the wide range of possibilities for theoretical analysis, QSR methods can play an important role in the characterization of new quantum optical states. It is hoped that the availability of these powerful methods will stimulate experimental efforts to generate new quantum states with non-Gaussian statistics using higher-order nonlinear processes.

Acknowledgments

The authors thank J. Mlynek for his constant support and encouragement, T. Müller, S. F. Pereira and J. P. Poizat for their collaboration in the initial stage of the experiment as well as A. Faridani and M. G. Raymer for providing the source code for the inverse Radon transform. We also acknowledge several fruitful discussins with R. Bruckmeier, W. P. Schleich, U. Leonhardt, G. M. D'Ariano and S. M. Tan. Partial financial support was provided by the Deutsche Forschungsgemeinschaft and the Esprit Long Term Research project No. 20029- ACQUIRE.

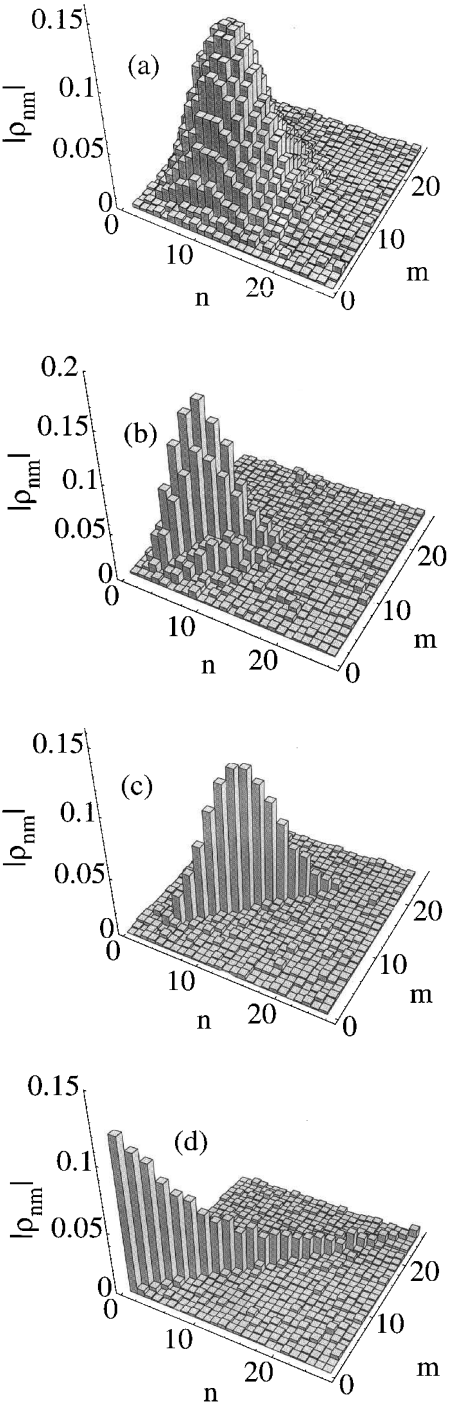

Figure 14. Reconstructed density matrices: (*a*) coherent state with purity $\mathrm{Tr}\,\rho^2 = 1$; (*b*) partially phase-diffused state with $\mathrm{Tr}\,\rho^2 = 0{\cdot}26$; (*c*) completely phase-diffused state with $\mathrm{Tr}\,\rho^2 = 0{\cdot}09$; (*d*) thermal sate with $\mathrm{Tr}\,\rho^2 = 0.079$. Owing to drifts of the signals' laser power, the average photon number of the state (*b*) is slightly smaller than those of the states (*a*) and (*c*).

References

[1] 1997, *J. mod. Optics*, this issue.
[2] Kimble, H. J., Dagenais, M., and Mandel, L., 1977, *Phys. Rev. Lett.*, **39,** 691; Short, R., and Mandel, L., 1983, *Phys. Rev. Lett.*, **51,** 384; Slusher, R. E., Hollberg, L. W., Yurke, B., Mertz, J. C., and Valley, J. F., 1985, *Phys. Rev. Lett.*, **55,** 2409; Wu, L.-A., Kimble, H. J., Hall, J. L., and Wu, H., 1986, *Phys. Rev. Lett.*, **57,** 691.
[3] Smithey, D. T., Beck, M., Raymer, M. G., and Faridani, A., 1993, *Phys. Rev. Lett.*, **70,** 1244.
[4] Smithey, D. T., Beck, M., Cooper, J., Raymer, M. G., and Faridani, A., 1993, *Phys. scripta* T, **48,** 35.
[5] Smithey, D. T., Beck, M., Cooper, J., and Raymer, M. G., 1993, *Phys. Rev.* A, **48,** 3159.
[6] Munroe, M., Boggavarapu, D., Anderson, M. E., and Raymer, M. G., 1995, *Phys. Rev.* A, **52,** R924.
[7] Breitenbach, G., Müller, T., Pereira, S., Poizat, J.-P.. Schiller, S., and Mlynek, J., 1995, *J. opt. Soc. Am.* B, **12,** 2304.
[8] Schiller, S., Breitenbach, G., Pereira, S. F., Müller, T., and Mlynek, J., 1996, *Phys. Rev. Lett.*, **77,** 2933; S. F. Pereita, G. Breitenbach, S. Schiller, and J. Mlynek, Les Houches lecture notes LXIII, (Elsevier).
[9] Breitenbach, G., Schiller, S., and Mlynek, J., 1997, *Nature*, **387,** 471.
[10] Vogel, K., and Risken, H., 1989, *Phys. Rev.* A, **40,** 2847.
[11] D'Ariano, G. M., Macchiavello, C., and Paris, M. G. A., 1994, *Phys. Rev.* A, **50,** 4298; Leonhardt, U., Munroe, M., Kiss, T., Richter, Th., and Raymer, M. G., 1996, *Optics Commun.*, **127,** 144.
[12] Leonhardt, U., and Raymer, M. G., 1996, *Phys. Rev. Lett.*, **76,** 1985; Richter, T., and Wünsche, A., 1996, *Phys. Rev.* A, **53,** R1974.
[13] Zucchetti, A., Vogel, W., Tasche, M., and Welsch, D.-G., 1996, *Phys. Rev.* A, **54,** 1; Banaszek, K., and Wodkiewicz, K., 1996, *Phys. Rev. Lett.*, **76,** 4344.
[14] Tan, S. M., *J. mod. Optics*, this issue, 2233.
[15] Royer, A., 1989, *Found. Phys.*, **19,** 3.
[16] Yuen, H. P., and Chan, V. W. S., 1983, *Optics Lett.*, **18,** 177.
[17] Collett, M. J., and Gardiner, C. W., 1984, *Phys. Rev.* A, **30,** 1386; Collett, M. J., and Walls, D. F., 1985, *Phys. Rev.* A, **32,** 2887.
[18] Polzik, E. S., Carri, J., and Kimble, H. J., 1992, *Appl. Phys.* B, **55,** 279; Kim, C., and Kumar, P., 1994, *Phys. Rev. Lett.*, **73,** 1605.
[19] Schneider, K., Bruckmeier, R., Hansen, H., Schiller, S., and Mlynek, J., 1996, *Optics Lett.*, **21,** 1396.
[20] Hong, C. K., and Mandel, L., 1985, *Phys. Rev. Lett.*, **54**, 323.
[21] Cahill, K. E., and Glauber, R. J., 1969, *Phys. Rev.*, **177,** 1882; Hillery, M., O'Connell, R. F., Scully, M. O., and Wigner, E. P., 1984, *Phys. Rep.*, **106,** 121.
[22] Leonhardt, U., and Paul, H., 1993, *Phys. Rev.* A, **48,** 4598; D'Ariano, G. M., Leonhardt, U., and Paul, H., 1995, *Phys. Rev.* A, **52,** R1801.
[23] Janicke, U., and Wilkens, M., 1995, *J. mod. Optics*, **42,** 2183.
[24] Schleich, W., and Wheeler, J. A., 1987, *Nature,* **326,** 574.
[25] Le Kien, F., Chizhov, A. V., Schleich, W. P., Breitenbach, G., Schiller, S., and Mylnek, J., 1997 (to be published).
[26] Dodonev, V. V., Man'ko, O. V., and Man'ko, V. I., 1994, *Phys. Rev.* A, **49,** 2993.
[27] Davidovich, L., 1996, *Rev. mod. Phys.*, **68,** 127.
[28] Kiss, T., Herzog, U., and Leonhardt, U., 1995, *Phys. Rev.* A, **52,** 2433.
[29] Lynch, R., 1995, *Phys. Rep.*, **256,** 368.
[30] Beck, M., Smithey, D. T., and Raymer, M. G., 1993, *Phys. Rev.* A, **48,** R890.
[31] Pegg, D. T., and Barnett, S. M., 1989, *Phys. Rev.* A, **39,** 1665.
[32] D'Ariano, G. M., 1996, *Proceedings of Quantum Communication and Measurement III*, Hakone, 1996.
[33] Schleich, W., Horowicz, R. J., and Varro, S., 1989, *Phys. Rev.* A, **40,** R7405.
[34] Arecchi, F. T., 1965, *Phys. Rev. Lett.*, **15,** 912.
[35] Raymer, M. G., Smithey, D. T., Beck, M., Anderson, M., and McAlister, D. F., *J. mod. Phys. B* (to be published).
[36] Loudon, R., 1973, *The Quantum Theory of Light* (Oxford University Press).
[37] Le Kien, F., Vogel, K., and Schleich, W. P., 1997, *Quant. semiclass. Optics*, **9,** 69.